AGU PUBLICATIONS

Geophysical Research Letters

RESEARCH LETTER
10.1002/2014GL060589

Key Points:
- K-H vortices observation under southward IMF
- Calculated vorticity normal to the spacecraft plain, and propagation estimate
- Circular induced electric field at the edges of the vortices perpendicular to B

Correspondence to:
G. Q. Yan,
gqyan@spaceweather.ac.cn

Citation:
Yan, G. Q., F. S. Mozer, C. Shen, T. Chen, G. K. Parks, C. L. Cai, and J. P. McFadden (2014), Kelvin-Helmholtz vortices observed by THEMIS at the duskside of the magnetopause under southward interplanetary magnetic field, *Geophys. Res. Lett.*, *41*, doi:10.1002/2014GL060589.

Received 21 MAY 2014
Accepted 10 JUN 2014
Accepted article online 16 JUN 2014

Kelvin-Helmholtz vortices observed by THEMIS at the duskside of the magnetopause under southward interplanetary magnetic field

G. Q. Yan[1], F. S. Mozer[2], C. Shen[1], T. Chen[1], G. K. Parks[2], C. L. Cai[1], and J. P. McFadden[2]

[1]State Key Laboratory of Space Weather, Center for Space Science and Applied Research, Chinese Academy of Sciences, Beijing, China, [2]Space Science Laboratory, University of California, Berkeley, California, USA

Abstract The Time History of Events and Macroscale Interactions during Substorms (THEMIS) observed several magnetopause crossings periodically at the duskside of magnetopause under southward interplanetary magnetic field (IMF), with significant sunward returning flows inside the magnetopause. The vortex features of the flows and the periodic enhancements in the calculated vorticity normal to the spacecraft plane could be found in the observation. The distortion of the magnetopause, the periodic features of vortex flows, the tailward propagation, and the evaluation of Kelvin-Helmholtz instability (KHI) condition support the evidence of the Kelvin-Helmholtz vortices produced by the velocity shear at the duskside of magnetopause. Based on three-point simultaneous observations of the flow, the vorticity was calculated to be about 0.15 s^{-1}, similar to previous results. The tailward propagation of the vortices along the flank magnetopause was estimated to be about 292 km/s. The circular-induced electric field of several mV/m was deduced perpendicular to the magnetic field when the magnetic field compression occurred at the edges of the vortices.

1. Introduction

There are many wavelike structures such as surface waves [*Sibeck*, 1992; *Mozer et al*., 1994] and Kelvin-Helmholtz (K-H) waves [*Chen and Kivelson*, 1993; *Kivelson and Chen*, 1995; *Fujimoto et al*., 2003; *Hasegawa et al*., 2004; *Foullon et al*., 2008] at the magnetopause boundaries. The K-H vortex is the nonlinear stage of one surface wave sandwiched between the two different regions with velocity shear. At the flanks side of the magnetopause, because the solar wind flows tailward and produces a shear with the stagnant magnetospheric plasma, it is amendable to excite the Kelvin-Helmholtz instability (KHI) and K-H waves. The nonlinear stage of the K-H surface wave could possibly cause the transport of solar wind into magnetosphere through the low-latitude boundary layer (LLBL). *Hasegawa et al*. [2004] found the evidence of the solar wind transport into the magnetosphere by the rolled-up K-H vortices under northward interplanetary magnetic field (IMF), in which the reconnection process was excluded due to the absence of predictable accelerated flows in the observation. However, the microphysical process that controls the solar wind transport into magnetosphere in the K-H vortices is still not clearly understood. *Nykyri and Otto* [2001] simulated the reconnection inside the vortices and estimated the transport efficiency across the magnetopause, which is a way for the solar wind in a reconnected magnetic island to be dispatched into magnetosphere. Recently, great effort has been made to find the observational evidence of such a reconnection process inside vortices, and some associated observations have been reported [*Nykyri et al*., 2006; *Eriksson et al*., 2009]. It was also emphasized that the model of reconnection inside vortices was different from the vortex-induced reconnection (VIR) model developed by *Liu and Hu* [1988] and *Liu and Pu* [1990a, 1990b]. By using the 2-D and 3-D models, respectively, *Nakamura et al*. [2006, 2008, 2013] simulated the reconnection induced in the vortices and compared the 3-D results with The Time History of Events and Macroscale Interactions during Substorms (THEMIS) observation. It was summarized that there were two types of the vortex-induced reconnection in 2-D [*Nakamura et al*., 2008]. In addition, *Faganello et al*. [2012] showed another type of the vortex-induced reconnection in 3-D. *Hasegawa et al*. [2009] revisited the Cluster event of rolled-up K-H vortices shown in *Hasegawa et al*. [2004] and found the evidence of the associated reconnection near the rolled-up interval. Some models or statistical studies presented that during northward IMF, the solar wind could be transported into magnetosphere through the LLBL caused by the KHI [*Fujimoto et al*., 1997; *Fairfield et al*., 2000; *Tsyganenko and Mukai*, 2003; *Yan et al*., 2005]. As for the single point observation of rolled-up vortices, the criteria were established [*Hasegawa et al*., 2006] to identify the rolled-up K-H vortices and the solar wind entry into the magnetosphere. The criteria can facilitate the observational analysis of K-H vortices.

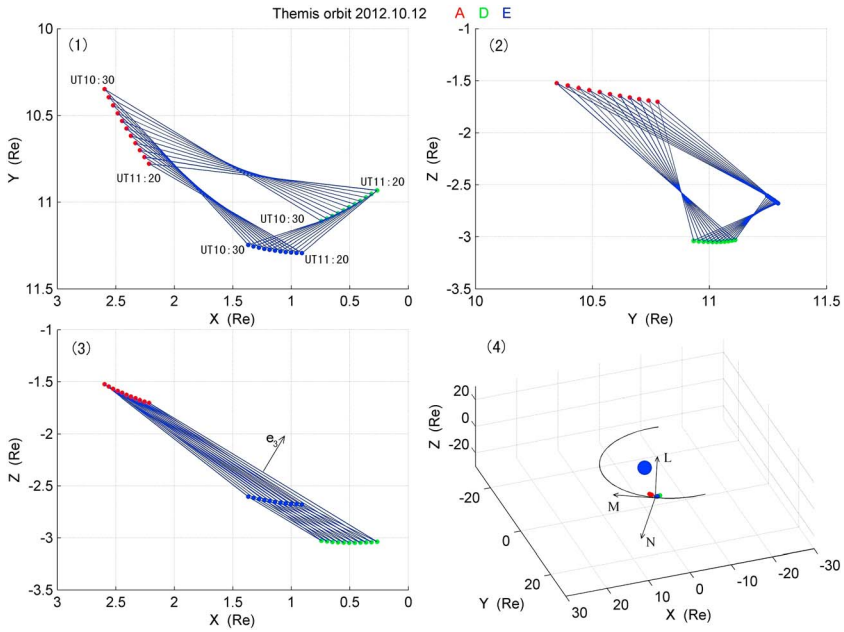

Figure 1. The orbits and positions of the TH-A in red, TH-D in green, and TH-E in blue, during the interested interval of UT 10:30 to UT 11:20, with the three-point triangle in blue lines every 5 min. The normal direction of the spacecraft plane $\boldsymbol{e_3}$ is presented in panel 3. The position data are expressed in GSM coordinates. The averaged local magnetopause coordinates LMN deduced from magnetopause model [*Shue et al.*, 1998] has been illustrated in panel 4.

The unstable condition for the KHI would not be changed by the sign of the IMF component perpendicular to the vortex plane, which roughly corresponds to the northward and southward component in the equatorial plane. The high density on both sides and the perpendicularity of the flow shear velocity to the undisturbed magnetic field can facilitate the excitation of KHI [*Hasegawa*, 1975]. On the other hand, it has been thought for a long time that the K-H waves were more preferentially excited [*Chen et al.*, 1997; *Farrugia et al.*, 2003; *Miura*, 1995; *Hashmoto and Fuijimoto*, 2005] and observed [*Chen and Kivelson*, 1993; *Kivelson and Chen*, 1995; *Fujimoto et al.*, 2003; *Hasegawa et al.*, 2004] under northward IMF. *Mozer et al.* [1994] investigated an observation of linear stage of surface waves observed by Geotail under southward IMF that were distorted less than 20°, by investigating the electric field. *Kawano et al.* [1994] also calculate the local normal direction of the magnetopause in the same event by using the minimum variance analysis (MVA). *Hwang et al.* [2011] reported the first observation of K-H vortices by Cluster at the dawnside of the magnetopause under southward IMF. To recapitulate, the current status is that most observations of K-H vortices are reported under northward IMF, and for southward IMF there is only one event reported by *Hwang et al.* [2011]. In this paper, we present another observation of the K-H vortices under southward IMF at the duskside of the magnetopause. This event shows the K-H vortices could also have noticeable periodicity and regularity under southward IMF. Moreover, a circular-induced electric field of several mV/m was found perpendicular to the magnetic field when the magnetic field compression occurred at the distorted magnetopause.

2. Orbits and Data

During the interval from UT 10:30 to UT 11:20 on 12 October 2012, the three spacecraft A, D, and E of THEMIS [*Angelopoulos*, 2008] were located at the duskside of the low latitude magnetopause with magnetic local time (MLT) about 18:00 and geocentric distances of 11 Re, forming a tilted triangle, as shown in Figure 1. Each of spacecraft crossed the magnetopause several times, which was distorted by the K-H vortices. In the analysis of this observation, we used the spin resolution measurements of about 3 s from the fluxgate magnetometer (FGM) [*Auster et al.*, 2008], the electrostatic plasma analyzer (ESA) [*McFadden et al.*, 2008], and the electric field instrument (EFI) [*Bonnell et al.*, 2008]. The ACE measurements at L1 point and FGM measurements on board TH-B at the lunar orbit (in the upstream solar wind with a 10 min time lag) were also used to confirm the southward IMF during the interval (Figure 2, panel 1).

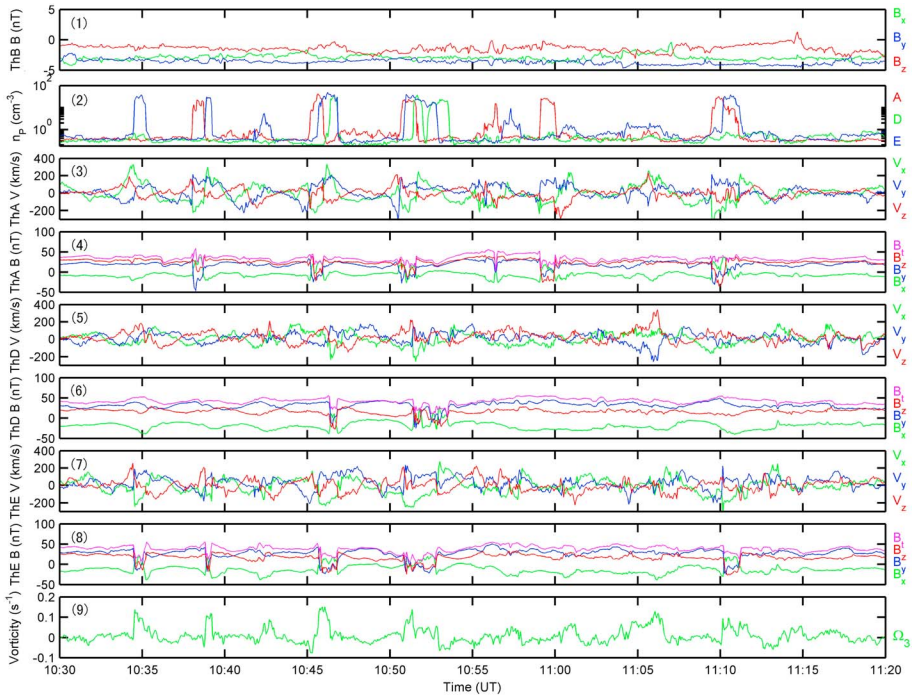

Figure 2. The periodical crossings of the flank side of the magnetopause by the three spacecraft of TH-A, TH-D, TH-E, and the vorticity normal to the three-point triangle plane. Panel 1 is the IMF monitored by ThB in the upstream solar wind at the Lunar orbit, with the about 10 min time lag; Panel 2 presents the ion densities in logarithmic plots observed by TH-A in red, TH-D in green, and TH-E in blue; in panel 3 are the velocity vectors from TH-A; in panel 4 are the magnetic field vectors from TH-A; in panel 5 are the velocity vectors from TH-D; in panel 6 are the magnetic field vectors from TH-D; in panel 7 are the velocity vectors from TH-E; in panel 8 are the magnetic field vectors from TH-E; panel 9 shows the vorticity normal to the three-point plane, calculated from the three-point simultaneous measurements of the velocity. All the vectors are expressed in GSM coordinates.

3. Observations and Discussion

Figure 2 shows observations from TH-A, TH-D, and TH-E. During the interval shown in Figure 2, the periodical crossings of magnetopause were observed 6 times by the TH-A, 2 times by TH-D, and 5 times by TH-E. For each crossing, when the spacecraft crossed the magnetopause into the magnetosheath, the ion density up to about 50–60 cm^{-3} in the magnetosheath and southward IMF were observed. On the other hand, when the spacecraft crossed the magnetopause back into the magnetosphere, the dilute and warm plasma and northward geomagnetic field could be seen, with significant sunward flows of 200–300 km/s. The three spacecraft formed a tilted triangle, as shown in the Figure 1, with the normal direction $\boldsymbol{e}_3$ of the spacecraft plane presented in panel 3. The ACE monitor showed the generally southward IMF and the solar wind velocity of 500 km/s at L1 (not shown). Furthermore, Artemis (THB and THC) in the upstream solar wind at the lunar orbit monitored the southward IMF (Figure 2, panel 1). Observations of southward IMF by the THEMIS spacecraft in the magnetosheath further confirmed that the IMF was southward for this time interval.

In Figure 2, the panels 3, 5, and 7, we present the velocity observations from TH-A, TH-D, and TH-E, respectively. The periodical features and the rotating of the flows could be seen in each single-point observation. The sunward flows inside the magnetopause and the tailward flows in the magnetosheath indicate the strong velocity shear at the magnetopause, which could excite the KHI and cause the vortices to propagate tailward along the magnetopause. The vortex flows can be illustrated by investigating the observed velocity in the averaged magnetopause coordinates LMN (Figure 3, panels 1, 2, and 3). The vectors in the M-N plane (approximately the vortex plane) showed the periodical features of vortices. The sunward returning flows inside the magnetopause were nearly the shear velocity in the magnetosheath, indicating that the sunward flows inside the magnetopause was caused by the rotation of the vortex flows. The time lags shown in panel 2 indicate the propagation from TH-A to TH-E, and then to TH-D. TH-D

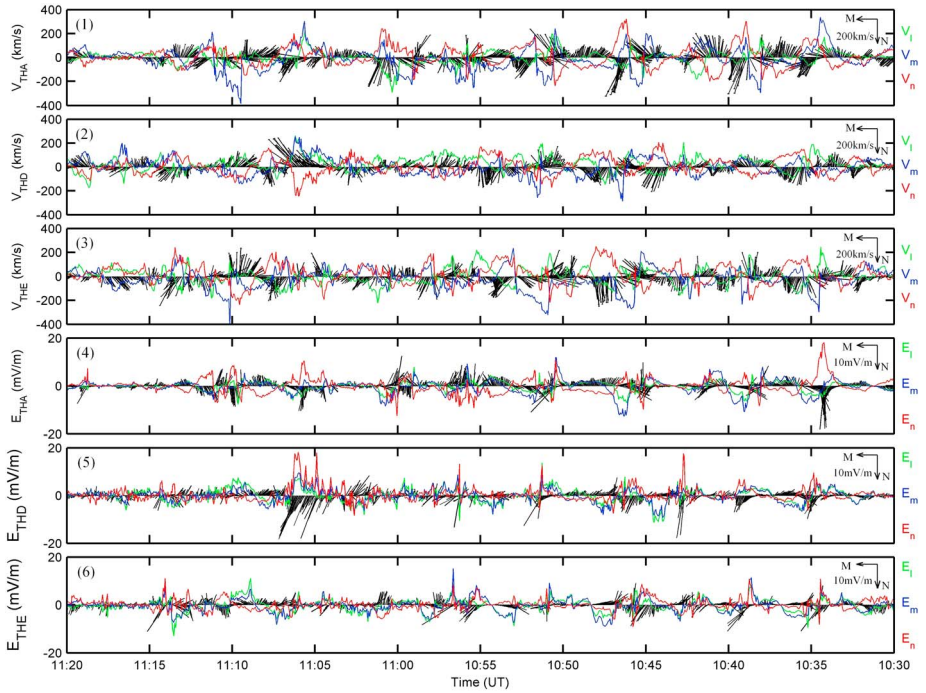

Figure 3. The vortex features in the velocity and electric field observation in LMN coordinates. In panel 1, panel 2, and panel 3, are V_l in green, V_m in blue, and V_n in red, observed by ESA on TH-A, TH-D, and TH-E, respectively; the black arrows present the velocity vectors in the vortex plane. In panel 1, panel 2, and panel 3 are E_l in green, E_m in blue, and E_n in red, observed by EFI on TH-A, TH-D, and TH-E, respectively; the black arrows present the electric field vectors in the vortex plane. All the vectors are expressed in averaged LMN coordinates, deduced from the magnetopause model by *Shue et al.* [1998].

crossed into magnetosheath only twice because it was located a little deeper inside the magnetosphere. The second crossing of TH-D appeared to show a split structure in both ion density observation (green line in panel 2) and magnetic field observation (panel 6). Although the split structure in the TH-D crossing could be also produced by magnetopause fluctuations, it could be more likely interpreted as the re-entry of the spacecraft into magnetosheath caused by the nonlinear, fully developed or rolled-up vortex, because such a structure was really one of the tailward propagating vortices as presented in Figures 2 and 3.

Shen et al. [2012] developed a new technique to calculate the spatial gradient based on three- to five-point measurements even when the space configuration is distorted, or even when only three-point measurements are available. In this particular event, the three spacecraft formed a tilted triangle with its normal direction $\boldsymbol{e}_3$ northward and a little tailward (Figure 1, panel 3). The separation between spacecraft was about 2 Re. The three-point configuration makes it possible to calculate the flow vorticity by using this technique. Only the component normal to the spacecraft plane could be calculated based on the three-point measurements in this event. There were ten periodical enhancements in the normal vorticity from UT 10:35 to UT 11:15 (Figure 2, panel 9), so the period was estimated about 4 min. The vorticity at the flank side of 18:00 MLT in this event is calculated as about 0.15 s^{-1}, similar to the 0.10 s^{-1} in the Cluster event at the flank side [*Hasegawa et al.*, 2004] that has been calculated by the same technique [*Shen et al.*, 2012]. The positive vorticity along the northward normal direction to the spacecraft plane is reasonable to the tailward velocity shear at the duskside of the magnetopause. The characteristic size of the spacecraft triangle is about $2\sqrt{w_1} = 13{,}000$ km (w_1 is the largest eigenvalue of the volume tensor). The calculated vorticity (Figure 2, panel 9) means that the vorticity could only be measured at such a size, so the vortex size (the size of flow rotation) should be estimated as 2 Re. By assuming that the K-H vortices propagate in the X-Y plane, i.e., $V_{pz} = 0$, the propagation speed could be estimated to be about 292 km/s with the azimuth angle of 150° in GSM coordinates, consistent with the tailward direction of magnetopause deduced from *Shue et al.* [1998] model, and similar to the propagation speed of about 320 km/s in *Hwang et al.* [2011] event. The wavelength (distance between the neighbor vortices) was

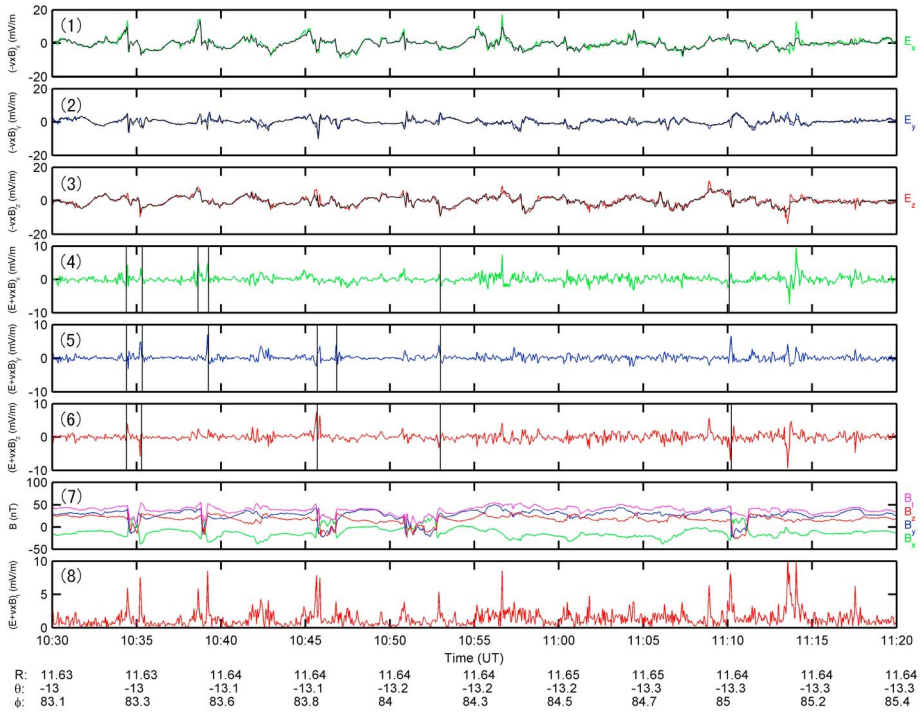

Figure 4. The comparison of the observed electric field with convective electric field in measurements of TH-E. In panel 1, panel 2, and panel 3 are E_x in green, E_y in blue, and E_z in red, respectively, observed by EFI on TH-E, and compared with the calculated three components of convective electric field $-\boldsymbol{v}\times\boldsymbol{B}$ in black lines; in panel 4, panel 5, and panel 6 are the three components of the induced electric field calculated as the difference between the observed electric field and the convective electric field, in green, blue, and red lines respectively; the observed magnetic field is shown in panel 7; the magnitude of the induced electric field is in panel 8. The bipolar signatures in the induced electric field were marked by vertical lines in panel 4, 5, and 6.

estimated to be about 11 Re. The number in the event of *Hwang et al*. [2011] was about 10 Re and typically was about a few 10^4 km in the Cluster observation [*Foullon et al*., 2008].

$$(\boldsymbol{k}\cdot\boldsymbol{V}_0)^2 > \frac{1}{\mu_0}\left(\frac{1}{\rho_1}+\frac{1}{\rho_2}\right)\left[(\boldsymbol{k}\cdot\boldsymbol{B}_1)^2+(\boldsymbol{k}\cdot\boldsymbol{B}_2)^2\right] \quad (1)$$

The unstable condition of the KHI (equation (1), $\boldsymbol{k}$ is the K-H wave vector, $\boldsymbol{V}_0$ is the shear velocity between the two regions, ρ_1 and ρ_2 are the mass densities of two regions, $\boldsymbol{B}_1$ and $\boldsymbol{B}_2$ is magnetic fields of the two regions respectively, and μ_0 is the permeability of vacuum) does not indicate a preference for northward or southward IMF, and the instability occurs more easily for a $\boldsymbol{k}$ vector perpendicular to the unperturbed magnetic field $\boldsymbol{B}_0$ [*Hasegawa*, 1975]. We evaluated the unstable condition in the averaged LMN coordinates, whose −M direction is the $\boldsymbol{k}$ direction. The averaged geomagnetic field and IMF observed by the spacecraft was, respectively, about $\boldsymbol{B}_m = [-13.43, -27.18, 20.96]$ and $\boldsymbol{B}_s = [7.72, -5.72, -9.13]$ nT in GSM, the observed densities in magnetosphere and magnetosheath were, respectively, about 1 cm^{-3} and 50 cm^{-3}, then the threshold of the shear velocity could be estimated as 203 km/s, easily surpassed by the tailward shear velocity of 200–300 km/s, so the unstable condition was satisfied in this event.

In the magnetic field measurements by each spacecraft (Figure 2, panels 4, 6, and 8), it is noticeable that there were enhancements in magnetic fields at the leading and trailing edges of the vortices, i.e., at the distorted magnetopause. Besides the enhancements, the crater type flux transfer event (FTE) [e.g., *Zhang et al*., 2010] or vortex-induced flux rope structures [e.g., *Nakamura et al*., 2013] were also possible within some individual vortex, but the periodicity is hard to be explained by the random FTEs. Most of the enhancements occurred in three components or two components, which is the feature of the magnetic field compression. When the vortex formed, the magnetosheath plasma was crushed into the magnetosphere and distorted the magnetopause. The wedge-like crush compressed the boundary layer and caused the time variance of the

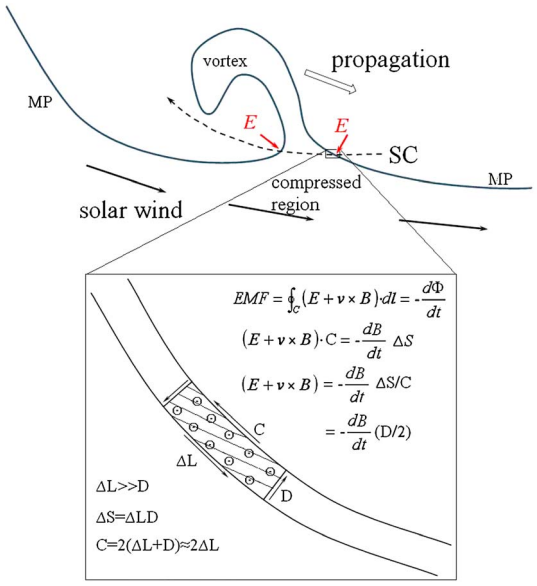

Figure 5. Illustration to estimate the induced electric field at the distorted magnetopause according to Faraday's Law. The closed circle line is chosen to be the rectangle at the compressed region at the edge of the vortex, with the direction shown in the figure.

magnetic field. According to Faraday's Law (equation (2)) [*Parks*, 2004], there should be induced electric field along the circles around the compressed magnetic field when the magnetic field compression occurs. If the induced electric field is strong enough, it should be measureable with bipolar signatures by the EFI.

$$EMF = \oint_C (\boldsymbol{E} + \boldsymbol{v} \times \boldsymbol{B}) \cdot d\boldsymbol{l} = -\frac{d\Phi}{dt} \quad (2)$$

We calculated the convective electric field $\boldsymbol{E}_{con} = -\boldsymbol{v} \times \boldsymbol{B}$ and compared it with the observed electric field. Only the observation from TH-E was presented (Figure 4, panels 1, 2, and 3) because similar features were found in the observations from TH-A and TH-D. One can see that it was quite consistent with the observed electric field, but there were still some difference at the edges of the vortices when the magnetic field compression occurred. The high consistencies between $\boldsymbol{E}_{con}$ and the observed electric field $\boldsymbol{E}$ indicated that the electric field comes mainly from the convective electric field at large scale. The difference between $\boldsymbol{E}_{con}$ and observed electric field only exists at small time scale.

The evidence of the K-H vortices could also be seen in the fluctuations of the observed electric field by each of the three spacecraft (colorful lines in Figure 4, panels 1, 2, and 3), because the orientation of the local magnetopause can be determined under the assumption that the main component of the electric field in the boundary layer is normal to the boundary [*Mozer et al.*, 1994]. When the magnetopause was distorted by the vortices, the boundary layer was also distorted, but the direction of electric field was maintained perpendicular to the magnetopause. That is why the fluctuations in electric field can be observed. At the same time, the electric field directions at the leading and trailing edges of one vortex should be predicted as illustrated by the red arrows in Figure 5. The observed electric field vectors in the M-N plane (nearly the vortex plane) by TH-A, TH-D, and TH-E have been plotted during the interested interval (Figure 3, panels 4, 5, and 6). The predicted electric field can be seen at leading and trailing edge of nearly each vortex. This feature means the magnetopause distortion by the K-H vortices. The directions of the electric field were rotating in the vortex plane, which could be interpreted as the rotating normal direction of the magnetopause. MVA is the alternative way to determine the normal direction of the magnetopause [e.g., *Hwang et al.*, 2011; *Kawano et al.*, 1994], but here we use the electric field.

FTE and vortex are not incompatible in this event. Under southward IMF, when the spacecraft crossed magnetopause, the southward IMF could clearly mark the crossings. The shift of magnetic field when spacecraft crossed magnetopause showed configuration changing from magnetosphere to magnetosheath or vice versa, less likely to be bipolar signatures characterizing the FTEs. If the FTE could explain the observed periodic features, the jets should have been observed mainly in V_l, which were not found in the observations. At the same time, FTE or flux rope was still possible to sporadically occur within an individual K-H vortex, but the periodic and propagating features were more likely the K-H vortices caused by the velocity shear because of the absence of the jets mainly in V_l/V_z and the absence of transient changing in magnetic field such as bipolar signatures in B_n; at least regular and periodic bipolar signatures were not found. On the other hand, the distortion of the magnetopause deduced from the electric field observation, the periodic features of the vortex flows observed by each spacecraft, and the tailward propagation from one spacecraft to the other, together with the evaluation of the K-H unstable condition, can support the K-H vortices in this event.

Furthermore, we removed $\boldsymbol{E}_{con}$ from the observed electric field to investigate the possible induced electric field $\boldsymbol{E}_{in} = \boldsymbol{E} - \boldsymbol{E}_{con} = \boldsymbol{E} + \boldsymbol{v} \times \boldsymbol{B}$. It is also the same reason that only the observation from TH-E was presented (Figure 4, panels 4, 5, and 6), because similar features can be observed by TH-A and TH-D. This removal of $\boldsymbol{E}_{con}$ is

equal to observe the electric field in a frame moving together with the frozen plasma and magnetic field, in which the convective electric field vanishes. At the edges of the K-H vortices, there existed significant induced electric field of several mV/m, distributed in each component when the magnetic field compression occurred. In the components of induced electric field, some bipolar signatures could be seen at the time marked by vertical lines (Figure 4, panels 4, 5, and 6). The bipolar signatures imply that the induced electric field should be circles around the compressed magnetic field, as predicted by Faraday's Law. The induced electric field $\boldsymbol{E_{in}} = \boldsymbol{E} + \boldsymbol{v} \times \boldsymbol{B}$ was calculated from the observation assuming that $\boldsymbol{E} \cdot \boldsymbol{B} = \boldsymbol{0}$. Note that non-convective electric field also satisfies that $\boldsymbol{E_{in}} \cdot \boldsymbol{B} = \boldsymbol{0}$. The induced electric field should also be in the perpendicular plane to magnetic field, which has also been predicted by Faraday's Law.

In order to estimate the induced electric field quantitatively, a closed rectangle in the vortex plane is chosen, as illustrated in Figure 5, and the induced electric field could be estimated as

$$\boldsymbol{E_{in}} = \boldsymbol{E} + \boldsymbol{v} \times \boldsymbol{B} = -\frac{d\boldsymbol{B}}{dt}(D/2) \tag{3}$$

The minus means that the $\boldsymbol{E}_{\text{in}}$ is along the opposite direction of the defined *C*. *D* is defined as the width of the compressed region, which could also approximately be the width of the LLBL, typically about 800–1000 km [*Happygood and Lockwood*, 1993; *Mozer et al*., 1994]. The observed $\frac{dB}{dt}$ at the compressed region could be typically about several nT/s, then the induced electric field caused by the magnetic field compression could be estimated as about several mV/m, consistent very well with the observation of $\boldsymbol{E} + \boldsymbol{v} \times \boldsymbol{B}$ (Figure 4, panel 8).

Based on the in situ observations, we can see that electric field comes mainly from the convective electric field at large scale, and there exists induced electric field generated by the compressed magnetic field at leading and trailing edges of the vortices. The electrons will be accelerated faster than protons by 1830 times in the circular electric field and then cause complex dynamic evolution. The induced electric field could be one of the possible factors to induce magnetic reconnection inside the K-H vortices or to cause other possible transport processes across the magnetopause, which would be investigated in further work.

4. Summaries

Generally, K-H vortices are observed under northward IMF, but *Hwang et al*. [2011] reported first observation under southward IMF on the dawnside of the magnetopause. In our work, the K-H vortices under southward IMF were observed by THEMIS at the duskside of the magnetopause. The results of our analysis could be summarized in three aspects: (1) under southward IMF, the K-H vortices can be accompanied by periodicity and regularity at the duskside of magnetopause, with significantly larger returning flows inside the magnetopause; (2) the distortion of the magnetopause, the periodic features of the vortex flows, the tailward propagation, and the evaluation of KHI condition imply that the vortices can be formed, with a tailward propagation of about 292 km/s; (3) the observed electric field mainly comes from convective electric field at large scale, and induced electric field of about several mV/m was deduced at the both leading and trailing edges of vortices when the magnetic field compression occurred. The bipolar signatures in the induced electric field imply that the induced electric field is circular around the compressed magnetic field, as predicted by Faraday's Law.

Acknowledgments
The data for this paper are available at the Coordinated Data Analysis Web of NASA's Goddard Flight Center (http://cdaweb.gsfc.nasa.gov/istp_public/). The Authors are grateful to the NASA's Goddard Flight Center and the associated instrument teams for supplying the data. This work was supported by the National Natural Science Foundation of China Grants 41004074, 41211120182, 40774081, and 41231066, and the Ministry of Science and Technology of China Grant 2011CB811404.

The Editor thanks two anonymous reviewers for assistance evaluating this manuscript.

References

Angelopoulos, V. (2008), The THEMIS mission, *Space Sci. Rev.*, *141*, 5–34, doi:10.1007/s11214-008-9336-1.
Auster, U., et al. (2008), The THEMIS fluxgate magnetometer, *Space Sci. Rev.*, *141*, 235–264, doi:10.1007/s11214-008-9365-9.
Bonnell, J. W., et al. (2008), The electric field instrument (EFI) for THEMIS, *Space Sci. Rev.*, *141*, 303–341.
Chen, Q., A. Otto, and L. C. Lee (1997), Tearing instability, Kelvin-Helmholtz instability, and magnetic reconnection, *J. Geophys. Res.*, *102*(A1), 151–161, doi:10.1029/96JA03144.
Chen, S. H., and M. G. Kivelson (1993), Nonsinusoidal waves at the magnetopause, *Geophys. Res. Lett.*, *20*(23), 2699–2702, doi:10.1029/93GL02622.
Eriksson, S., et al. (2009), Magnetic island formation between large-scale flow vortices at an undulating postnoon magnetopause for northward interplanetary magnetic field, *J. Geophys. Res.*, *114*, A00C17, doi:10.1029/2008JA013505.
Faganello, M., F. Califano, F. Pegoraro, T. Andreussi, and S. Benkadda (2012), Magnetic reconnection and Kelvin-Helmholtz instabilities at the Earth's magnetopause, *Plasma Phys. Control. Fusion*, *54*(12), 124037, doi:10.1088/0741-3335/54/12/124037.
Fairfield, D. H., A. Otto, T. Mukai, S. Kokubun, R. P. Lepping, J. T. Steinberg, A. J. Lazarus, and T. Yamamoto (2000), Geotail observations of Kelvin-Helmholtz instability at the magnetotail boundary for parallel northward field, *J. Geophys. Res.*, *105*(A9), 21,159–21,173, doi:10.1029/1999JA000316.

Farrugia, C. J., F. T. Gratton, R. B. Torbert, L. Bender, G. Gnavi, K. W. Ogilvie, N. V. Erkaev, R. P. Lepping, and P. Stauning (2003), On the dependence of dayside Kelvin-Helmholtz activity on IMF orientation, *Adv. Space Res.*, *31*, 1105–1110.

Foullon, C., C. J. Farrugia, A. N. Fazakerley, C. J. Owen, F. T. Gratton, and R. B. Torbert (2008), Evolution of Kelvin-Helmholtz activity on the dusk flank magnetopause, *J. Geophys. Res.*, *113*, A11203, doi:10.1029/2008JA013175.

Fujimoto, M., T. Terasawa, and T. Mukai (1997), The cold-dense plasma sheet: A GEOTAIL perspective, *Space Sci. Rev.*, *80*, 325–339.

Fujimoto, M., T. Tonooka, and T. Mukai (2003), Vortex-like fluctuations in the magnetotail flanks and their possible roles in plasma transport, in *the Earth's Low-Latitude Boundary Layer*, *Geophys. Monogr. Ser.*, vol. 133, edited by P. T. Newell and T. Onsager, p. 241, AGU, Washington, D. C.

Happygood, M., and M. Lockwood (1993), On the voltage and distance across the low-latitude boundary layer, *Geophys. Res. Lett.*, *20*, 145–148, doi:10.1029/93GL00063.

Hasegawa, A. (1975), *Plasma Instabilities and Non-Linear Effects*, Springer, New York.

Hasegawa, H., M. Fujimoto, T.-D. Phan, H. Rème, A. Balogh, M. W. Dunlop, C. Hashimoto, and R. TanDokoro (2004), Transport of solar wind into Earth's magnetosphere through rolled-up Kelvin-Helmholtz vortices, *Nature*, *430*, 755.

Hasegawa, H., M. Fujimoto, K. Takagi, Y. Saito, T. Mukai, and H. Rème (2006), Single-spacecraft detection of rolled-up Kelvin-Helmholtz vortices at the flank magnetopause, *J. Geophys. Res.*, *111*, A09203, doi:10.1029/2006JA011728.

Hasegawa, H., et al. (2009), Kelvin-Helmholtz waves at the Earth's magnetopause: Multiscale development and associated reconnection, *J. Geophys. Res.*, *114*, A12207, doi:10.1029/2009JA014042.

Hashmoto, C., and M. Fuijimoto (2005), Kelvin-Helmholtz instability in an unstable layer of finite thickness, *Adv. Space Res.*, *37*, 527–531.

Hwang, K.-J., M. M. Kuznetsova, F. Sahraoui, M. L. Goldstein, E. Lee, and G. K. Parks (2011), Kelvin-Helmholtz waves under southward interplanetary magnetic field, *J. Geophys. Res.*, *116*, A08210, doi:10.1029/2011JA016596.

Kawano, H., S. Kokubun, Y. Yamamoto, K. Tsuruda, H. Hayakawa, M. Nakamura, T. Okada, A. Matsuoka, and A. Nishida (1994), Magnetopause characteristics during a four-hour interval of multiple crossings observed with GEOTAIL, *Geophys. Res. Lett.*, *21*(25), 2895–2898, doi:10.1029/94GL02100.

Kivelson, M. G., and S. H. Chen (1995), The magnetopause: Surface waves and instabilities and their possible dynamic consequences, in *Physics of the Magnetopause*, *Geophys. Monogr. Ser.*, vol. 90, edited by P. Song, B. O. Ü. Sonnerup, and M. F. Thomsen, p. 257, AGU, Washington, D. C.

Liu, Z. X., and Y. D. Hu (1988), Local magnetic field reconnection caused by vortices in the flow field, *Geophys. Res. Lett.*, *15*(8), 752–755, doi:10.1029/GL015i008p00752.

Liu, Z. X., and Z. Y. Pu (1990a), The model of vortex-induced reconnection, I, Dynamic characters, *Acta Geophys. Sin.*, *33*, 1.

Liu, Z. X., and Z. Y. Pu (1990b), The model of vortex-induced reconnection, II, Theory and simulation of flux transfer events, *Acta Geophys. Sin.*, *33*, 250.

McFadden, J. P., C. W. Carlson, D. Larson, M. Ludlam, R. Abiad, B. Elliott, P. Turin, M. Marckwordt, and V. Angelopoulos (2008), The THEMIS ESA plasma instrument and in-flight calibration, *Space Sci. Rev.*, *141*, 277–302, doi:10.1007/s11214-008-9440-2.

Miura, A. (1995), Dependence of the magnetopause Kelvin-Helmholtz instability on the orientation of the magnetosheath magnetic field, *Geophys. Res. Lett.*, *22*(21), 2993–2996, doi:10.1029/95GL02793.

Mozer, F. S., H. Hayakawa, S. Kokubun, M. Nakamura, T. Okada, T. Yamamoto, and K. Tsuruda (1994), The morningside low-latitude boundary layer as determined from electric field and magnetic field measurements on Geotail, *Geophys. Res. Lett.*, *21*(25), 2983–2986, doi:10.1029/94GL01296.

Nakamura, T. K. M., M. Fujimoto, and A. Otto (2006), Magnetic reconnection induced by weak Kelvin-Helmholtz instability and the formation of the low-latitude boundary layer, *Geophys. Res. Lett.*, *33*, L14106, doi:10.1029/2006GL026318.

Nakamura, T. K. M., M. Fujimoto, and A. Otto (2008), Structure of an MHD-scale Kelvin-Helmholtz vortex: Two fluid simulations including finite electron inertial effects, *J. Geophys. Res.*, *113*, A09204, doi:10.1029/2007JA012803.

Nakamura, T. K. M., W. Daughton, H. Karimabadi, and S. Eriksson (2013), Three-dimensional dynamics of vortex-induced reconnection and comparison with THEMIS observations, *J. Geophys. Res. Space Physics*, *118*, 5742–5757, doi:10.1002/jgra.50547.

Nykyri, K., and A. Otto (2001), Plasma transport at the magnetospheric boundary due to reconnection in Kelvin-Helmholtz vortices, *Geophys. Res. Lett.*, *28*(18), 3565–3568, doi:10.1029/2001GL013239.

Nykyri, K., A. Otto, B. Lavraud, C. Mouikis, L. M. Kistler, A. Balogh, and H. Rème (2006), Cluster observations of reconnection due to the Kelvin-Helmholtz instability at the dawnside magnetosphere flank, *Ann. Geophys.*, *24*, 2619–2643, doi:10.5194/angeo-24-2619-2006.

Parks, G. K. (2004), *Physics of Space Plasmas: An Introduction*, Westview Press, Boulder, Colo.

Shen, C., et al. (2012), Spatial gradients from irregular multiple point spacecraft configurations, *J. Geophys. Res.*, *117*, A11207, doi:10.1029/2012JA018075.

Shue, J.-H., et al. (1998), Magnetopause location under extreme solar wind conditions, *J. Geophys. Res.*, *103*, 17,691–17,700, doi:10.1029/98JA01103.

Sibeck, D. G. (1992), Transient events in the outer magnetosphere: Boundary waves or flux transfer events?, *J. Geophys. Res.*, *97*(A4), 4009–4026, doi:10.1029/91JA03017.

Tsyganenko, N. A., and T. Mukai (2003), Tail plasma sheet models derived from Geotail particle data, *J. Geophys. Res.*, *108*(A3), 1136, doi:10.1029/2002JA009707.

Yan, G. Q., et al. (2005), A statistical study on correlations between plasma sheet and solar wind based on DSP explorations, *Ann. Geophys.*, *23*, 2961–2966.

Zhang, H., et al. (2010), Evidence that crater flux transfer events are initial stages of typical flux transfer events, *J. Geophys. Res.*, *115*, A08229, doi:10.1029/2009FA015013.